ACS chemical biology

ARTICLES

pubs.acs.org/acschemicalbiology

Immobilizing Reporters for Molecular Imaging of the Extracellular Microenvironment in Living Animals

Zuyong Xia,[†] Yun Xing,[†] Jongho Jeon,[†] Young-Pil Kim,[†,#] Jessica Gall,[†] Anca Dragulescu-Andrasi,[†] Sanjiv S. Gambhir,[†,‡,∥] and Jianghong Rao[†,§,⊥,*]

[†]Molecular Imaging Program at Stanford, Department of Radiology & Bio-X Program, Departments of [‡]Bioengineering, [§]Chemistry, and [∥]Materials Science and Engineering, and [⊥]Biophysics and Cancer Biology Programs, Stanford University, 1201 Welch Road, Stanford, California 94035-5484, United States

Supporting Information

ABSTRACT: We report here an immobilization strategy using a collagen binding protein to deliver and confine synthetic reporters to the extracellular microenvironment *in vivo* for noninvasively imaging the activity of targets in the microenvironment. We show that the immobilization of reporters on collagens in the local microenvironment is highly efficient and physiologically stable for repetitive, long-term imaging. By using this strategy we successfully developed an immobilized bioluminescent activatable reporter and a dual-modality reporter to map and quantitatively image the activity of extracellular matrix metalloproteinases (MMP) in tumor-bearing mice. The inhibition of MMP activity by chemical inhibitor was also demonstrated in living subjects. We further demonstrated the general applicability of this immobilization strategy by imaging MMP activity at the inflammation site in a mouse model. Our results show that the *in vivo* immobilization of reporters can be used as a general strategy for probing the local extracellular microenvironment.

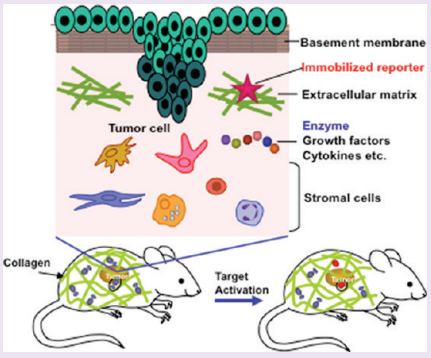

The microenvironment as an integral part of cells plays critical roles in their physiology, structure, and function. There are continuously increasing interests in understanding how the microenvironment controls the behavior and fate of stem cells[1,2] and the initiation, progression, and metastasis of tumors.[3−5] Molecular characterization of the extracellular microenvironment is usually performed *in vitro* through identification of the secreted proteins in cultured cells[6] and analysis of gene expression in purified components of normal and malignant tissues.[7] The great complexity of the extracellular microenvironment and our current incomplete understanding of the biological factors involved present a big challenge in recreating an *ex vivo* counterpart. *In vivo* imaging can shed light into the biological processes within their native microenvironment through tracking the movement of cells genetically labeled with fluorescent proteins.[8−14] It is, however, presently challenging to directly image specific signaling molecules in the extracellular microenvironment involved in the cell-to-cell and cell-to-matrix interactions because of the lack of methods that can stably present the designed reporters in the extracellular microenvironment *in vivo*. To meet this critical need, we report here a simple, general strategy to deliver and immobilize synthetic reporters for creating a reporting system in animals for *in vivo* imaging of molecular signaling and interactions in the microenvironment.

Our strategy takes advantage of the ubiquitous distribution of collagen proteins, which are a major component of the extracellular matrix inside the mammalian body. Collagens provide an ideal harbor for the reporters because of their abundance (they are the most abundant proteins in the body, representing about 30% of total proteins) and relative physiological stability. In our design, a reporter is immobilized onto the collagens in extracellular microenvironment through a collagen-binding protein (Figure 1a). Unlike targeting to the cell surface, which often leads to internalization of the reporters, binding of the reporters to collagens will prevent them from being internalized into cells and retain them in the extracellular microenvironment for effective sensing. With this strategy we were able to create a mouse with reporters embedded throughout the body. The distribution, stability, and function of the immobilized reporters were evaluated by successfully mapping extracellular enzyme activity in tumor-bearing mice. We further evaluated the immobilized reporter for imaging enzyme activity in an inflammation site in a mouse model to demonstrate the general applicability of the reporter immobilization strategy for various biological models.

RESULTS

***In Vivo* Immobilization with Collagen Binding Protein CNA35.** CNA35, a 35 kDa collagen binding domain in an adhesion protein from *Staphylococcus aureus*,[15] binds a variety of collagen types with high affinity (K_d ~500 nM) and has been used for *in vitro* collagen visualization.[16−18] We first evaluated the

Received: April 27, 2011
Accepted: August 10, 2011
Published: August 10, 2011

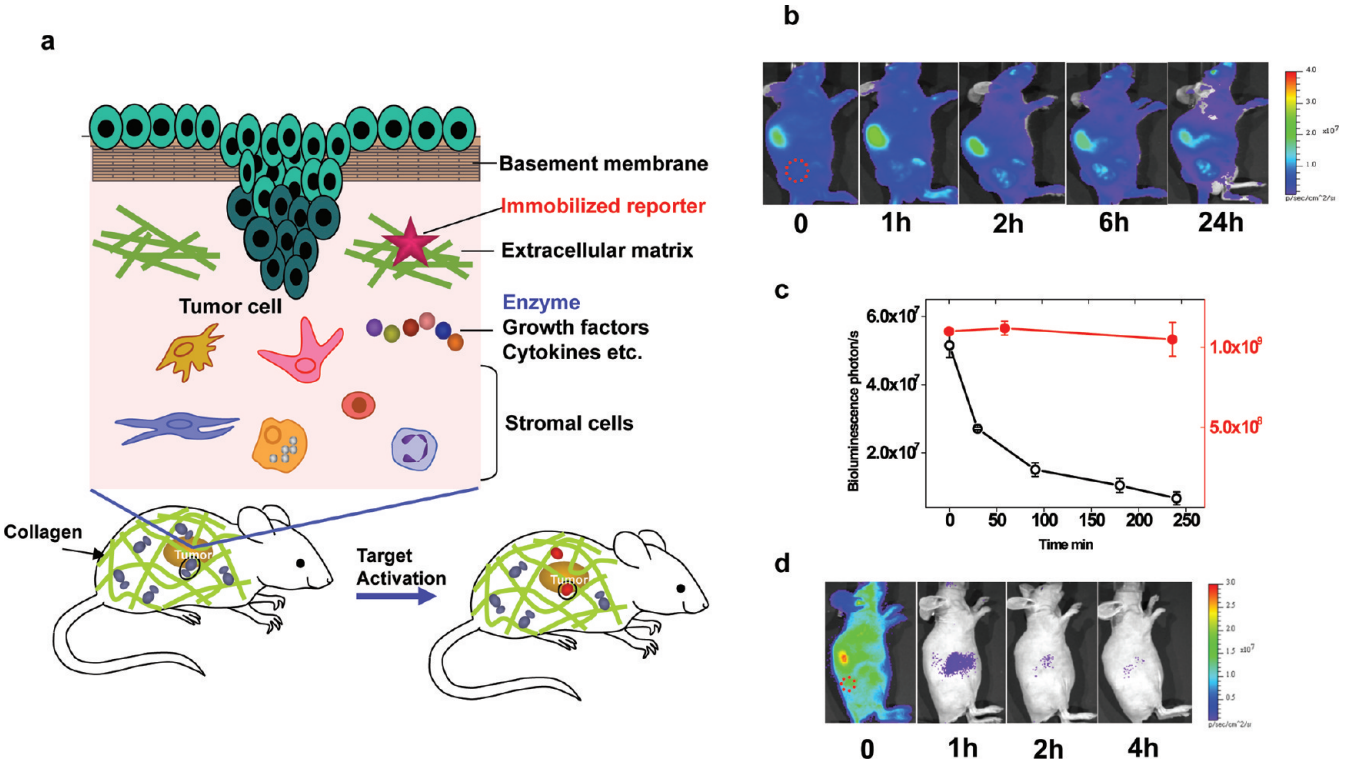

Figure 1. A reporter immobilization strategy for *in vivo* imaging. (a) Schematic of reporter immobilization over the body through binding ubiquitous collagens for imaging the extracellular microenvironment. (b) *In vivo* bioluminescence imaging of CB-Luc, a fusion reporter of Luc8-535 with CNA35 in nude mice with HT1080 tumor xenografts (marked by a red circle). The reporter protein (10 pmol) was injected *via* the tail vein (acquisition time, 1 s; 10 μg coelenterazine). The liver showed the highest bioluminescence emission, and the biodistribution of the reporter activity in tissues at 24 h post-injection is shown in Supplementary Figure 1. (c) Plot of the bioluminescence emission in the whole body (red dot; right *y*-axis) and in blood (black open circle; left *y*-axis) at various post-injection time points. (d) Fast clearance of nonimmobilized Luc8-535 from the circulation after injection into nude mice with HT1080 tumor xenografts (red circle).

reporter-immobilizing ability of CNA35 by using a bioluminescence reporter, which can be sensitively monitored because of extremely low background bioluminescence. Luc8-535, an engineered mutant of *Renilla* luciferase that emits maximally at 535 nm and has excellent chemical and biological stability (more than 200 h of half-life in mouse serum),[19,20] was genetically fused with the N-terminus of CNA35. The luciferase activity of the purified Luc8-535 and CNA35 fusion protein (CB-Luc, collagen binding luciferase) was approximately 60% of that of Luc8-535. CB-Luc (10 pmol) was injected *via* the tail vein into a nude mouse with a xenograft HT1080 tumor and imaged at different intervals with intravenous injection of the substrate of *Renilla* luciferase, coelenterazine. During the first 4 h, the total intensity of the bioluminescence emission throughout the mouse body decreased less than 5% (Figure 1b). However, the bioluminescence in the blood dropped 50% in 30 min and 88% in 4 h (Figure 1c). The observation of fast clearance of CB-Luc from the blood compared to practically no decrease in the total bioluminescence emission suggests that the binding of CB-Luc to the collagen proteins *in vivo* is relatively fast and that the immobilization is highly efficient. The binding of the CB-Luc to collagen was remarkably stable *in vivo*. After 24 h, the total bioluminescence intensity from the mice remained 60% of the initial value, and 8 days post-injection, more than 10% of signal (more than 20% after the correction of the biochemical half-life of Luc8-535 activity in mouse serum) remained (Supplementary Figure 1a). As a comparison, the same amount of Luc8-535 (without CNA35) gave a strong initial emission after injection (Figure 1d), but the total emission decreased by 55-fold in just one hour, and less than 1% of the initial signal remained after 4 h. The biodistribution study of CB-Luc in mice sacrificed at 4 h post-injection revealed the presence of the fusion protein reporter in all organs (Supplementary Figure 1b). A further study with radiolabeled reporters provided more quantitative information on their biodistribution and stability (Supplementary Figure 2). Consistent with the result of the bioluminescence imaging, the biodistribution of the radiolabeled reporter remained essentially unchanged in the majority of organs and tissues even after 24 h except for the liver and kidneys, which showed an approximate 50% decrease, probably due to the degradation and clearance of the fusion protein reporter. Notably, the reporter concentration in blood was low even at the initial one hour, indicating fast extravasation of the reporter and rapid binding with the collagens. These results demonstrate highly efficient immobilization of the reporters through collagen binding and good *in vivo* stability of immobilized reporters.

The specific binding of CB-Luc to the collagens was verified by histological staining of the tumor tissue samples. The CB-Luc was labeled with the fluorescent dye Cy5 and injected into the tumor-bearing mice through the tail vein. After 24 h the tumor samples were collected, frozen, and sectioned for immunostaining of the collagens. The collagen type I antibody was used as the primary antibody for staining of the type I collagen because the collagen binding protein CNA35 has the highest affinity for the

dx.doi.org/10.1021/cb200135e |*ACS Chem. Biol.* 2011, 6, 1117–1126

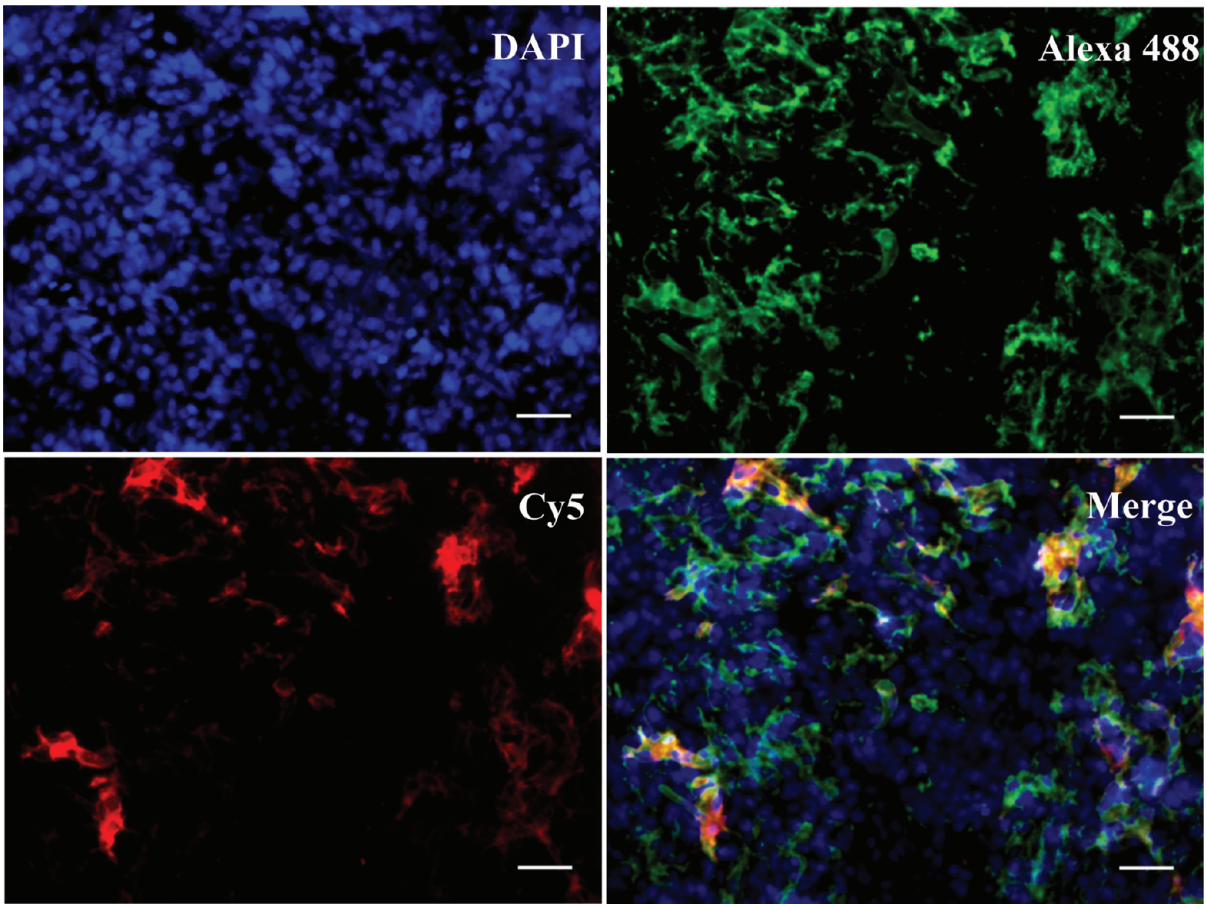

Figure 2. Histological analysis of binding of CB-Luc to collagens in tumor. The Luc8-535 and collagen binding protein CNA35 fusion protein CB-Luc was labeled with Cy5 (excitation, 650 nm; emission:, 670 nm). The tumor tissues were collected 24 h after iv injection of 0.5 nmol of Cy5-labeled CB-Luc. The frozen tissue sections were stained with primary collagen type I antibody and Alexa 488 conjugated secondary antibody (Alexa 488: excitation, 499 nm; emission, 519 nm). The Cy5-labeled CB-Luc (red) co-localizes well with type I collagen (green), indicating the accumulation of CB-Luc on the type I collagen after 24 h. Scale bar: 50 μm.

type I collagen. The collagens were visualized by a secondary antibody conjugated with Alexa 488, and the CB-Luc was directly imaged by the conjugated Cy5 (Figure 2). Nearly all of the red fluorescence signal from CB-Luc co-localized with the green fluorescence signal from the type I collagens in the tumor tissue sections (Figure 2) verified that the CB-Luc is likely bound and accumulated on the type I collagens *in vivo*.[15]

Bioluminescent Activatable Reporter for MMP Sensing. Having proven the ubiquitous distribution and good stability of the immobilized reporters, we next applied the strategy to immobilize reporters for imaging specific targets in the extracellular microenvironment. One of the important components within the extracellular microenvironment are secreted enzymes, such as matrix metalloproteinases (MMPs), that process many molecular targets including growth factors and extracellular matrix proteins and are overexpressed in a variety of tumors.[21,22] We first chose gelatinases matrix metalloproteinase-2 and 9 (MMP-2/9) as the model target in the tumor extracellular microenvironment to evaluate our *in vivo* reporter immobilization strategy for imaging the microenvironment.

Fluorescent probes have been developed for *in vivo* imaging of enzyme activity,[23−25] but there have been no successful examples of activatable bioluminescent reporters yet for *in vivo* imaging of enzyme activity.[26] The extremely high sensitivity and low background of bioluminescent reporters presents a large advantage for *in vivo* imaging. We hypothesized that an activatable bioluminescent reporter could be designed by attaching chemical dye quenchers to a bioluminescent protein. Bioluminescence resonance energy transfer (BRET) from the bioluminescent protein to the dye quenchers should result in a quenched dark state,[27,28] and the removal of the quenchers by MMP-2 would restore the bioluminescent emission (Figure 3a).

We used dabcyl, a non-emitting absorber, as the quencher since its absorption spectrum shows a good degree of overlapping with the emission spectrum of Luc8-535 (Figure 3b). Dabcyl was chemically conjugated to the MMP-2 substrate peptide (GPLGVRGC, also a substrate of MMP-9, which usually shares the same substrate specificity as MMP-2)[23,24] at the N-terminus (Supplementary Figure 3). A heterobifunctional linker containing both an NHS ester and maleimide ($SM(PEG)_4$) was used to conjugate the peptide *via* its cysteine side chain to the side chains of lysine residues on the fusion protein reporter CB-Luc. As shown in Figure 3c, when the NHS ester of the dabcyl-peptide (16 μM) conjugate was added to CB-Luc (8 μM), the bioluminescent emission of CB-Luc dropped drastically. The bioluminescent emission of the reporter was able to be restored by MMP-2. Figure 3d shows the activation kinetics of a reporter (1.0 μM) with on average 4 quenchers per CB-Luc in the presence of MMP-2 (160 nM) over

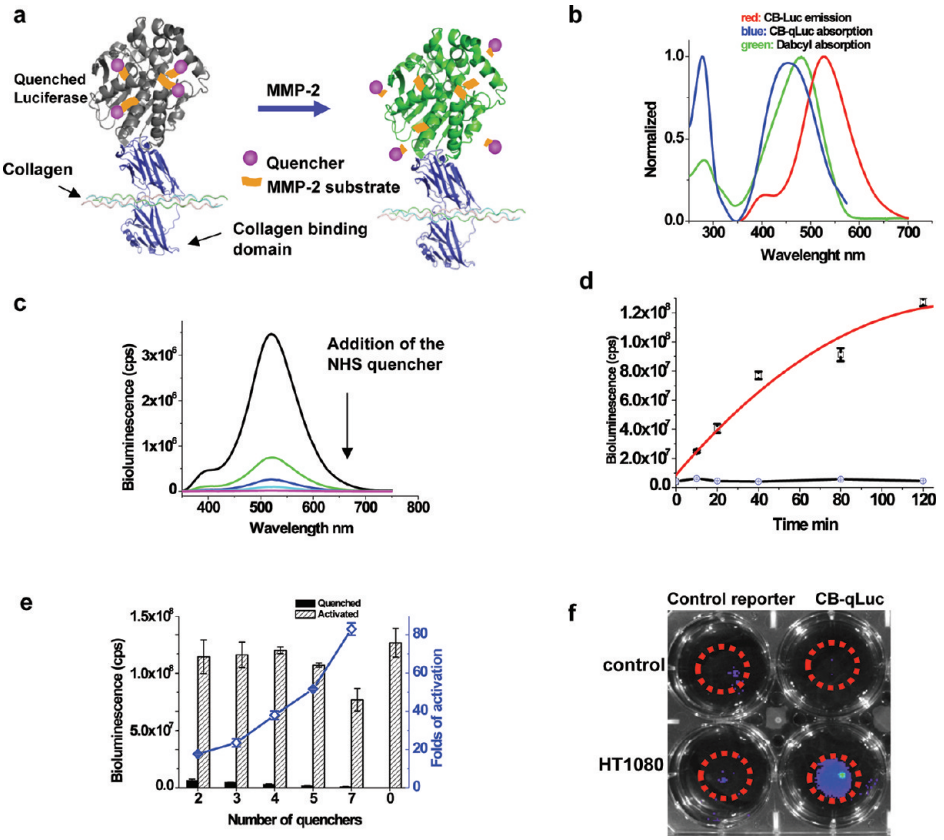

Figure 3. Characterization of bioluminescent activatable reporter CB-qLuc for mapping MMP-2/9 activity in living mice. (a) Design of bioluminescent reporter CB-qLuc for sensing MMP-2/9 activity. (b) Emission spectrum of CB-Luc and absorption spectra of dabcyl and dabcyl-conjugated CB-qLuc. (c) Bioluminescence emission spectrum of CB-Luc (8 μM in 200 μL of PBS buffer, pH 7.4) after a stepwise addition of the NHS ester of dabcyl-conjugated MMP-2/9 substrate every 15 min over the course of 1 h. The amount of the quencher in the solution increases from the top to bottom: 0, 2, 4, 6, and 8 equiv; typically 4 quenchers are conjugated to CB-Luc at the end of the reaction. (d) Activation kinetics of quenched CB-qLuc (red) and the scrambled control reporter (black) (1.0 μM; 4 quenchers per protein on average) by recombinant MMP-2 (160 nM) in 0.05% Tween-20 PBS buffer (pH 7.4) at 37 °C. (e) Effect of the number of quenchers on the luciferase activity of CB-qLuc before and after MMP-2 activation for 2 h under the same condition as in panel d. (f) Imaging MMP-2/9 activity in cell culture with 10 pmol of CB-qLuc (right row) or scrambled probe (left row) immobilized in 50 μL of matrigel at the center of the dishes (marked by red circles). HT1080 cells (50% confluence) were cultured for 12 h before bioluminescence imaging, and no cells were in the control dishes.

the course of 2 h. As a comparison, the control reporter with a scrambled MMP-2 substrate sequence (GVRLGPGC) could not be activated by MMP-2. As expected, the quenching efficiency was dependent on the number of quenchers conjugated to the protein. The contrast ratio of the emission before and after the MMP-2 activation was 18-, 24-, 38-, 51-, and 82-fold for 2, 3, 4, 5, and 7 quenchers per CB-Luc, respectively (Figure 3e).

CB-qLuc was tested for imaging the MMP activity in the HT1080 culture medium containing secreted MMP-2 and 9. Both CB-qLuc (with 4 quenchers on average) and the control reporter were added to the culture dishes containing HT1080 cells and the control dishes without HT1080 cells but only the medium and matrigel for a period of 12 h incubation (Figure 3f). The bioluminescent emission from the control reporter in the HT1080 cell dish was about 20% higher than that from the control dish, but 200% higher bioluminescent emission was observed with CB-qLuc in the HT1080 cell dish than that in the control dish. This result demonstrates that our activatable bioluminescent reporter can image the activity of extracellular MMP-2/9 secreted by HT1080 cells *in vitro*.

***In Vivo* Mapping of Local MMP Activity in Tumors.** The MMP reporter CB-qLuc tested above was then evaluated in living mice for imaging the MMP activity. A nude mouse with an HT1080 tumor xenograft received 11 pmol of CB-qLuc *via* the tail vein injection (Figure 4a). At different time intervals, 10 μg of coelenterazine was injected intravenously prior to image acquisition. A time-dependent increase in the bioluminescent emission was observed at the tumor site. The activation of CB-qLuc at the tumors was small at the early time points but could still be visualized due to the high signal-to-noise ratio with the bioluminescence imaging (image at 1 h in Figure 4a). Among the more than 20 mice imaged, all of the tumors displayed increased emission 1 h post-injection of CB-qLuc, and at 24 h, the contrast between the tumor site and normal tissues near the tumor site increased significantly to 8.6 $\pm$ 0.2 ($P < 0.01$, $n = 4$). Continuous activation of CB-qLuc by MMP was observed 6 days post-injection (Supplementary Figure 4). For the immobilized control reporter under the same conditions, no significant bioluminescent emission was detected throughout the body in the first 6 h (Figure 4b), and after 24 h, the contrast between the tumor site and the normal tissue near the tumor site increased slightly to 2.1 $\pm$ 0.3 ($P < 0.01$, $n = 4$). Tumors were excised and lysed for *in vitro* zymographic analysis (Supplementary Figure 5), confirming the presence of active MMP-2 in tumors (14.8 $\pm$ 1.6 ng/mg protein

dx.doi.org/10.1021/cb200135e |*ACS Chem. Biol.* 2011, 6, 1117–1126

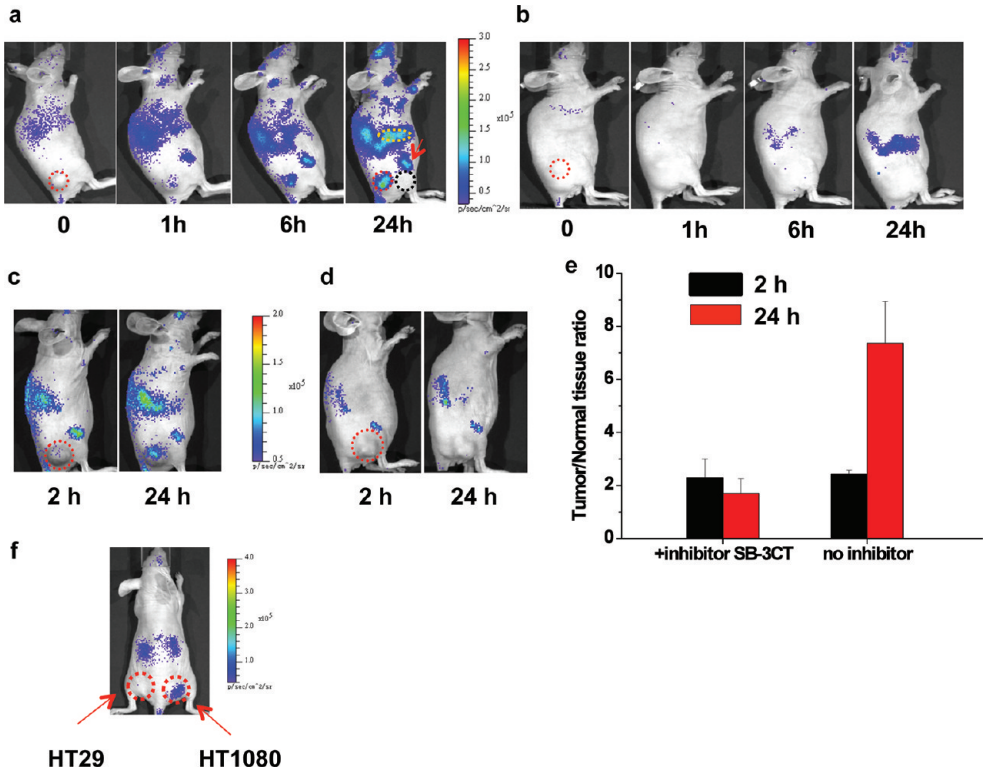

Figure 4. Immobilizing reporters for imaging MMP-2/9 activity and its inhibition in tumor xenografts. (a,b) Representative bioluminescence images of mice with xenografted HT1080 tumors. An 11 pmol quantity of (a) CB-qLuc or (b) a control reporter was iv injected into each mouse. At indicated time points after the reporter injection, 10 μg of coelenterazine was iv injected for each image collection (acquisition time, 20 s). Tumors are marked by red circles. The tissue near the tumor (black dash circle) is selected for comparison. The liver is indicated with a yellow circle, and one of the joints by a red arrow. (c−e) Imaging the inhibition of MMP-2/9 activity *in vivo*: (c) without and (d) with SB-3CT (500 μg, ip injected 2 h before iv injection of 10 pmol of CB-qLuc); 10 μg of coelenterazine was iv injected for each image collection (acquisition time, 10 s). (e) Quantification of the MMP-2/9 activity from the images in the inhibition study. The *y*-axis is the bioluminescence ratio between the tumor and normal tissue near the tumor. For mice without inhibitor treatment in panel c, the ratios are 2.4 ± 0.1 and 7.4 ± 1.5 at 2 and 24 h, respectively ($P < 0.02$, $n = 3$); for inhibitor-treated mice in panel d, the ratios are 2.3 ± 0.7 (2 h) and 1.7 ± 0.5 (24 h) ($P < 0.02$, $n = 3$). (f) Imaging MMP-2/9 activity in HT1080 and HT29 (control) cells implanted in mice; 2 × 10^7 cells were injected subcutaneously into nude mice. A 10 pmol quantity of CB-qLuc was injected through tail vein. The right image shows bioluminescence 4 days after cell implantation. The HT1080 implantation site shows 7.6 ± 1.6 ($P < 0.01$, $n = 2$) fold higher bioluminescence intensity than the HT29 site. Red circles mark the tumors as indicated.

tissue, an average of 6 mice). These results demonstrate that our activatable bioluminescent reporter has been successfully immobilized *in vivo* and can image the MMP activity at the tumor microenvironment.

Notably, significant signals were also detected at other sites besides the tumors, for example, the joints at the front and back legs and the liver (Figure 4a). For the control reporter with the scrambled MMP substrate sequence, only slightly increased emission was detected in the liver at the same time point. These data suggest that the immobilized reporter can map the local enzyme activity throughout the whole body of the animal. The observation of considerable MMP activity in other tissues and organs compared to the tumors also emphasizes the need for stable immobilization of the reporters for truly imaging the local microenvironment.

We confirmed the specific activation of the reporter by MMP in an inhibition study using SB-3CT an inhibitor that is relatively specific to MMP-2/9. SB-3CT irreversibly inhibits the enzyme activity by forming a covalent adduct (K_i for MMP-2 is 14 nM, and 600 nM for MMP-9).[29,30] The inhibitor was intraperitoneally injected to HT1080 tumor-bearing mice 2 h before iv injection of the CB-qLuc. We observed almost complete inhibition of the activation of CB-qLuc with injection of 500 μg of SB-3CT (Figure 4d). The bioluminescence ratio between the tumor site and the surrounding normal tissue slightly decreased from 2.3 ± 0.7 at 2 h to 1.7 ± 0.5 at 24 h post-injection of CB-qLuc ($P < 0.02$, $n = 3$) (Figure 4e). In addition, no significant increase in bioluminescence of the whole animal was observed after treatment with the inhibitor. On the other hand, the continuous increase of the bioluminescence signal at the tumor site and with the whole animal was observed in the mice without the inhibitor treatment: the tumor/surrounding tissue ratio increased to 7.4 ± 1.6 at 24 h from 2.4 ± 0.1 at 2 h ($P < 0.02$, $n = 3$) (Figure 4c).

Further evidence showing the specific activation of the reporter CB-qLuc by MMP-2/9 *in vivo* was obtained from differential imaging of two tumor cell lines HT1080 and HT29 implanted in the same mice. HT29 cells secrete very low levels of active MMP-2/9.[31] Our previous *in vitro* assay of the MMP-2 activity in the HT29 cell culture showed more than 10-fold lower MMP-2 activity than that in HT1080 cell culture.[32] We subcutaneously implanted both HT29 and HT1080 in the same mouse. The CB-qLuc reporter was injected intravenously right after the tumor cell implantation. This experiment also examined if the immobilization strategy could work in disease models where the EPR

dx.doi.org/10.1021/cb200135e |*ACS Chem. Biol.* 2011, 6, 1117–1126

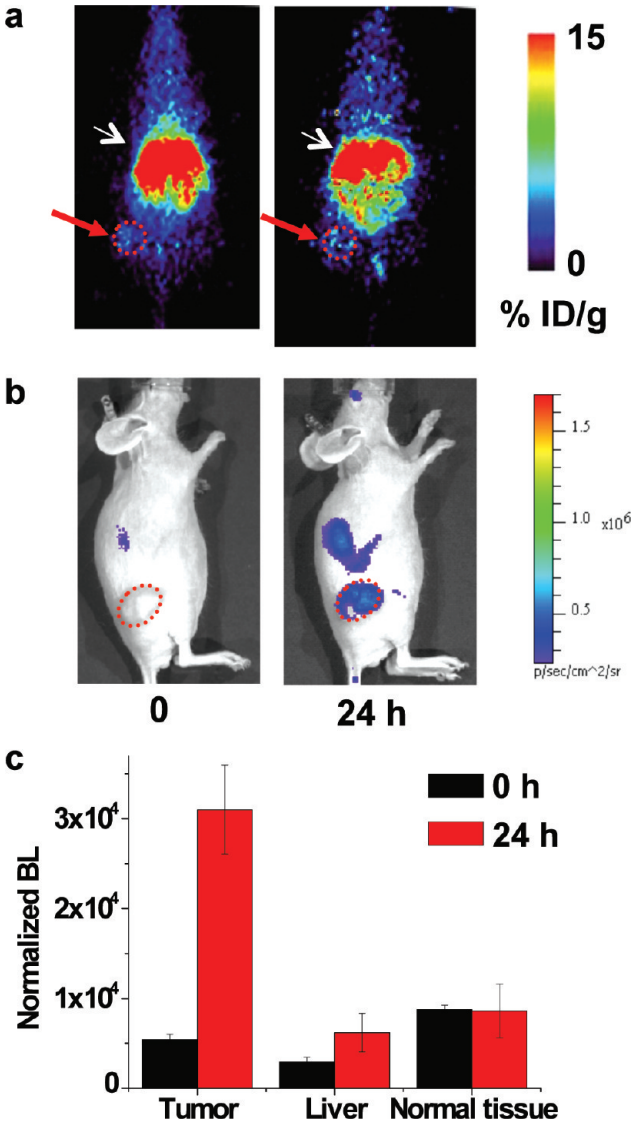

Figure 5. Immobilization of a dual-modality reporter for quantitative imaging of MMP-2 activity. (a) PET imaging with ^{64}Cu-labeled CB-qLuc reporter (coronal view); 90 μCi of reporters (120 μL, 1.2 μM in PBS) were iv injected, and static scans were acquired at 0 and 24 h. White arrows indicate the liver, and red arrows mark the tumor location. (b) Bioluminescence imaging acquired immediately after the PET scans. Note that the imaging position of the mouse is different from the PET images in panel a for better tumor visualization; tumors are marked by a red circle. (c) Quantification of the MMP-2 activity in different regions. The bioluminescence signal before (0 h) and after (24 h) activation of the reporters was normalized to the reporter concentration (as determined by PET) in the selected regions. The normalized bioluminescence was calculated by dividing the average radiance obtained from bioluminescence imaging by the average probe concentration obtained from PET imaging at each site. The fold-activation at 24 h is 5.5 $\pm$ 0.2 (n = 3, P < 0.02) at the tumor site, 2.2 $\pm$ 1.1 (n = 3, P < 0.05) at the liver, and 1.0 $\pm$ 0.3 (no activation) at the normal tissue near the tumor.

(enhanced permeability and retention) effect does not exist. Since the CB-qLuc reporter was injected before the formation of a solid tumor mass, there was no accumulation of the reporters at the cell implantation sites through the EPR effect. The injected CB-qLuc was found to stay long enough for monitoring the enzyme activity at the cell implantation sites. Significant activation of the CB-qLuc at the HT1080 site 4 days after implantation and injection of the CB-qLuc reporter was observed (Figure 4f). The bioluminescence from the HT1080 implantation site was 7.6 $\pm$ 1.6 (P < 0.01, n = 2) fold higher than that from the HT29 implantation site. The selective imaging of the MMP activity from HT1080 but not HT29 cells implanted in the same mouse further suggests that the CB-qLuc is likely activated by MMP-2/9.

Quantitative Imaging of the MMP Activity with ^{64}Cu-Labeled CB-qLuc. Since the concentration of the reporter may vary in tissue locations, quantitative analysis of the enzyme activity requires simultaneous determination of the concentrations of both the substrate (the reporter) and the product (activated reporter). We addressed this need by introducing a second imaging modality, positron emission tomography (PET),[33] to quantify the total reporter concentration. We labeled CB-qLuc with ^{64}Cu, a positron-emitting isotope, and on average one DOTA-^{64}Cu ligand was conjugated to each reporter CB-qLuc *via* its amino groups. The uptake of the dual functional reporter is high in liver, kidneys and spleen (Supplementary Figure 2). There is no statistically significant difference in the tumor uptake over 24 h: 1.7 $\pm$ 0.3% ID/g tissue at 1 h, 1.8 $\pm$ 0.4% at 4 h, and 1.5 $\pm$ 0.5% (n = 4) at 24 h.

After PET imaging (Figure 5a), the mice were immediately transferred to the cooled CCD imaging system (Figure 5b). We selected three regions for comparison of their MMP-2/9 activity: liver, tumor and its nearby superficial normal tissues. The concentration of the total reporter at each selected region was estimated from the PET signals and used to normalize the bioluminescence signal. At the beginning (t = 0 h), the observed residual bioluminescence signals are due to the residual Luc8-535 activity (Figure 5c). The normalized bioluminescence signal (independent of the reporter concentration) at time zero would be the same at different regions if there was no depth-dependent attenuation of the bioluminescent light, and their difference reflects the depth of the location of the immobilized reporters. Indeed, at time zero, the normalized bioluminescence values decrease in the order of normal nearby superficial tissue, tumor, and liver as the tissue depth increases (Figure 5c); it is worth noting that without the PET normalization the bioluminescence signal at the liver was the highest. After 24 h, the normalized bioluminescence signal from the tumor increased by 5.5 $\pm$ 0.2 fold (n = 3, P < 0.02) (Figure 5c), whereas no changes were observed with the tissue near the tumor. The normalized bioluminescence signal from the liver increased by 2.2 $\pm$ 1.1 fold (n = 3, P < 0.05) in comparison to that at the time zero. With an immobilized dual functional reporter, MMP activity at different regions can be quantitatively imaged.

***In Vivo* Imaging of MMP Activity in an Inflammation Model.** Unlike other receptor-targeted imaging approaches, the unique feature of the reporter immobilization strategy is that the reporters are retained in the local tissues and no accumulation of the reporters or specific binding to the target molecules is required. In a second disease model, we evaluated the immobilization strategy for imaging enzyme activity at the inflammation site of a living mouse.

Matrix proteolysis is a hallmark of the inflammatory process, and MMPs as matrix-degrading proteases play important roles in inflammation. The increased or mis-regulated levels of many MMPs are observed in diseases associated with inflammation.[34,35] In addition to degrading matrix, MMPs are also found to act as

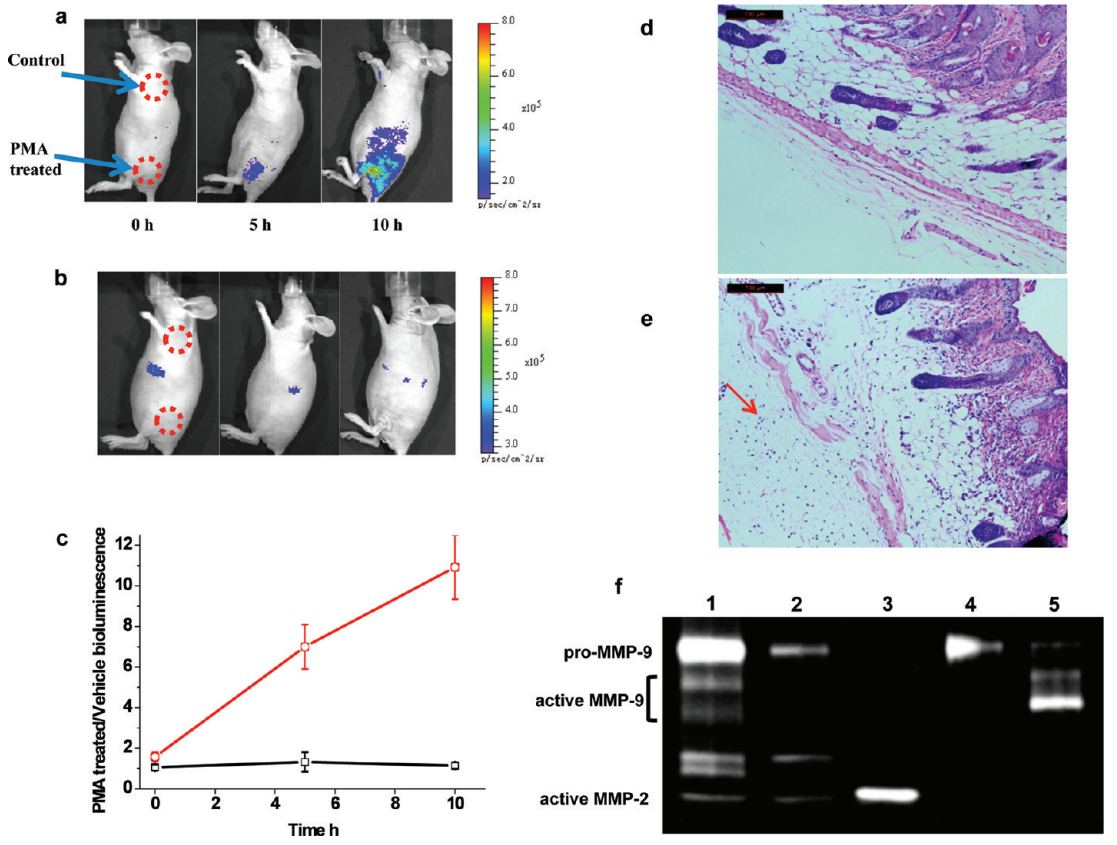

Figure 6. Imaging the MMP-9 activity in the inflammation site of a living mouse. (a) To induce inflammation, phorbol 12-myristate 13-acetate (PMA) (10 μg in acetone) was topically applied on the low left flank of the mice three times in a week. The same volume acetone was applied on the shoulder as the control. qCB-Luc (10 pmol) was iv injected, and coelenterazine (10 μg) was iv injected before imaging (exposure time, 20s). (b) MMP activity imaging after an ip injection of 500 μg of inhibitor SB-3CT 2 h before the injection of the MMP reporter. (c) Plot of the ratio of activated bioluminescence at the inflammation sites over the control sites without (red curve) and with (black curve) the ip injection of SB-3CT. The skin samples were collected for H & E staining after imaging: (d) cross-section of the normal skin and (e) skin of the inflammation site with extensive infiltration of neutrophils (indicated by a red arrow) and the destruction of the tissue. (f) Gelatin zymography analysis of the homogenized skin samples shows elevated MMP-9 activity in the inflamed skin. Lane 1, PMA-treated skin sample; Lane 2, vehicle-treated skin sample; Lane 3, active MMP-2 standard; Lane 4, pro-MMP-9 standard; Lane 5, activated MMP-9 by incubation of pro-MMP-9 with 1 mM of 4-aminophenylmercuric acetate at 37 °C for 30 min.

effectors in various processes. The ability to monitor *in vivo* MMP activity in real time will help to reveal their roles in diseases involving inflammation. Here we show that CB-qLuc can directly image MMP activity in a cutaneous inflammation model.

Inflammation can be induced by topically applying PMA (phorbol myristate acetate) onto the mouse's skin.[36] MMP-2/9 are the major MMPs that are overexpressed at the inflammation site.[37,38] After multiple topical applications of PMA on the nude mouse skin, 10 pmol of CB-qLuc was iv injected. Strong bioluminescence signal emitted from the PMA-treated skin site, and the contrast to the vehicle-treated skin site reached 10.9 ± 1.6 fold in 10 h (Figure 6a,c). The activation of the reporter CB-qLuc was faster and more significant in comparison to that in tumor imaging, suggesting a much higher level of MMP activity during the inflammation process. The specific activation of the reporter by MMPs was similarly confirmed by ip administration of SB-3CT: no significant activation of the reporter was observed in 10 h, and the bioluminescence emission from the PMA- and vehicle-treated skin sites were at the same level (Figure 6b,c). At the end of the bioluminescence imaging experiments, the skin samples were collected for histological analysis. In comparison to the vehicle-treated skin, the PMA-treated skin showed characteristics of inflammation including the presence of massive neutrophil infiltrates and tissue destruction in the dermis due to the matrix degradation by MMPs (Figure 6d,e). Gelatin zymography analysis of the skin tissue lysates revealed that the level of MMP-9 dramatically increased in the inflammation skin, while the increase in the level of MMP-2 was much less than MMP-9 (Figure 6f). These results demonstrate that the reporter immobilization strategy can image the enzyme activity during inflammation in living mice. We observed predominant activation of the reporters at the inflammation site, suggesting a much higher level of MMP-9 activity than other regions. The enzyme activity can be similarly quantitated with a dual-modality reporter as in the tumor imaging.

DISCUSSION

We have developed an *in vivo* immobilization strategy for systemic delivery of reporters to visualize the molecular targets in the extracellular microenvironment. Collagens were chosen as the base for immobilization because of their abundance in the extracellular matrix and the extremely small amount of reporters introduced (typically tens of pmol) should have minimal interference on their normal physiological function. The reporters immobilized on collagens are ubiquitously distributed in the

dx.doi.org/10.1021/cb200135e |*ACS Chem. Biol.* 2011, 6, 1117–1126

body and retained for a long period of time. Importantly, the binding of the reporters to collagens will prevent them from being internalized into cells and retain them extracellularly for long-term imaging. The protease-activatable reporters on collagens are well exposed and fully functional in the extracellular microenvironment of tumors and in the cutaneous inflammation site. The immobilization strategy offers an attractive solution to characterizing the extracellular microenvironment *in vivo* because it can provide local information on specific targets in the microenvironment and also allows global mapping of the target activity in the whole body for comparison.

The MMP activity is usually analyzed in the tissue samples. However, with the *in vitro* analysis it is hard to assess the exact MMP activity under *in vivo* conditions due to tight regulation of the enzyme activity by the endogenous effectors such as tissue inhibitors of metalloproteinases (TIMPs).[39,40] The variations on tissue sample preparation also limit accurately assessment of the enzyme activity in the different tissues.

A number of activatable probes have been previously reported for *in vivo* imaging of enzyme activity in tumors.[23−25] These probes preferentially accumulate at the tumor sites by taking advantage of the leaky tumor vasculature through the EPR effect. A potential problem of this type of probes is that they can also be activated by the enzyme present in other regions besides the tumor site, and the activated products may eventually translocate and accumulate in tumors, also through the EPR effect, as reported in a recent study.[40] These issues make it difficult to reliably quantify the enzyme activity in tumors with the EPR based activatable probes. Furthermore, these probes will not be useful for studying other disease models where the EPR effect does not exist. Neither of these issues is a limiting factor for the collagen-based reporter immobilization strategy.

We observed slow activation of MMP reporters in the xenografted HT1080 tumor (Figure 4). The zymogram of the tumor lysate, however, showed that over 50% of MMP-2 was in the active form (Supplementary Figure 5). Since the MMP activity is regulated by both the expression control and TIMP inhibition, it is thus likely that most of active MMP-2 in the tumor microenvironment was inhibited by TIMPs. For example, TIMP-1 inhibits MMP-mediated degradation of extracellular matrix[41] and can also stimulate cell growth[42] and inhibit apoptosis.[43] In accompanying with the increased MMP expression in HT1080 cells, there may be a local increase in the TIMPs expressed from tumor or neighboring stroma cells to maintain the balance between the tumor growth and matrix degradation. This argument is consistent with the dual roles TIMPs play in the modulation of MMP activity: they are necessary to assist activation of pro-MMPs but also inhibit the MMP activity.[44]

In the inflammation model, a burst of MMP-9 activation in the inflammation model was observed shortly after the injection of the reporters (Figure 6a). On the other hand, the zymogram of the tissue lysates showed that the proportion of active MMPs was much lower than that in the tumor (Figure 6f). It is thus likely that the MMP activity regulation in the inflammation site may be different from the tumor and that there may not be an increased TIMPs expression. In light of the dual role of TIMPs in the modulation of MMP activity,[44] like MMP-2, pro-MMP9 may similarly require TIMPs for its activation.

As an enzyme that catalyzes the hydrolysis of its substrates, both concentrations of the product and substrate have to be determined for quantitative imaging of the MMP activity. Previous activatable MMP probes measure only the signal from the product-activated probe.[23−25] Since the probe is often not evenly distributed after systematic introduction into the body, without prior knowledge of the amount of the probe localized at the tumor, it can result in over- or under-estimating the enzyme activity from only the activated product signal. Therefore, a second imaging modality should be introduced to provide an independent, quantitative measurement of the reporter (both activated and nonactivated) concentration at all of the tissues. The signal resulting from activated reporter is normalized against the total concentration determined from the PET imaging, and the normalized value thus truly reflects the MMP activity. For example, the MMP activity in the liver appeared as high as in the tumor before the normalization (Figure 4a), but after the normalization of the reporter concentration, the MMP activity in the liver is much lower than that in the tumor (Figure 5c). This result underscores the important consideration in designing and applying activatable probes for quantitative imaging enzyme activity *in vivo*.

In summary, we have imaged the enzymatic activity of gelatinases in the extracellular microenvironment with immobilized activatable reporters and demonstrated its general applicability for *in vivo* imaging extracellular microenvironment in two disease models. Reporters for sensing other molecular targets and events of interest may be similarly immobilized for the microenvironment imaging. The fact that many growth factors are present at very low concentrations in the microenvironment may also require activatable reporters with a mechanism of signal amplification for sensitive detection. We anticipate that the reporter immobilization will be a general strategy for long-term serial real-time imaging of biological targets in the microenvironment at the molecular level.

METHODS

Materials. Dabcyl NHS ester was from Anaspec (San Jose, CA). Cy5 was from GE Healthcare. Bifunctional linker, succinimidyl-([*N*-maleimidopropionamido]-4-ethyleneglycol) ester ($SM(PEG)_4$) was from Pierce. Coelenterazine was from Nanolight (Pinetop, AZ). Rink amide resins for peptide synthesis were from Novabiochem. Active recombinant MMP-2 was from Calbiochem. Pro-MMP-9 was from Anaspec. Collagen type I antibody from rabbit was from AbCam. Alexa 488 conjugated antirabbit IgG from goat was from invitrogen. SB-3CT was from Enzo Life Sciences. Bioluminescence emission spectra were collected on a FluoroMax-3 (Jobin Yvon Inc.) with the excitation light blocked, and emission spectra were corrected with a correction file provided by the company. TD-20/20 luminometer (Turner Biosystems) was also used for characterization of the quenched bioluminescent reporters.

***In Vivo* MMP Activity Imaging in the Tumor.** Tumor xenografts were generated by injecting 5×10^6 HT1080 cells subcutaneously in the back flank of athymic nude or SCID mice (6 weeks old, Charles River). Images were typically collected on IVIS 200 (Xenogen Inc.). One to two weeks after the tumor implantation with mice anesthetized with 2% isofluorane, CB-qLuc (10−100 pmol) was iv injected to the tumor-bearing mice. Luciferase substrate coelenterazine was iv injected at the time of imaging. The concentration of probes in circulation was monitored by measuring bioluminescence in 5 μL of blood samples withdrawn periodically. For imaging MMP-2/9 activity right after the tumor cell implantation, 2×10^7 HT29 and HT1080 cells were subcutaneously injected. CB-qLuc (10 pmol) was iv injected right after the cell implantation. For biodistribution studies of CB-Luc, organs were harvested after imaging. Tissue lysates at a concentration of 100 mg/mL were prepared in 2.5% Triton X-100, 25 mM Tris buffer (pH 7.5 and

300 mM NaCl). The bioluminescence in 200 μL of lysate was measured with an IVIS 200 imager.

***In Vivo* MMP Inhibition Study in the Tumor.** The inhibitor SB-3CT (500 μg) in 200 μL of PBS buffer was intraperitoneally injected into the mice with HT1080 tumors. After 2 h, CB-qLuc (10 pmol) was iv injected and imaged 2 and 24 h later.

MicroPET and Bioluminescence Imaging. MicroPET imaging was performed on a GE Vista scanner. The anesthetized animals were placed in a imaging chamber, positioned on the scanner bed, ^{64}Cu labeled CB-qLuc (90 μCi, 1.2 μM in 120 μL of PBS buffer) was injected *via* tail vein, and a static whole-body PET scan was acquired at 0, 1, 4, and 24 h after injection. Immediately after the microPET scan, mice were iv injected with coelenterazine and imaged at the IVIS Spectrum (Xenogen Inc.). The reporter concentration in various tissues was determined by using the AMIDE software.[45] The bioluminescence was analyzed by Living Imaging 3.2 from Caliper. The regions of interest (ROIs) from the PET imaging were calculated from an ellipsoid ROI drawn over the selected organs and tissues. The mean values were directly used as the average reporter concentration in the selected regions. The average radiance (photon/s/cm^2/sr) of selected ROIs from bioluminescence imaging was normalized to the average probe concentration of the same region from PET.

***In Vivo* MMP Activity Imaging in the Inflammation.** To induce inflammation, 10 μg of PMA in 100 μL of acetone was topically applied on the mouse skin every 2 days. Acetone was applied as control. After 1 week, 10 pmol of CB-qLuc was iv injected. For inhibition study, mice were ip injected with 500 μg of SB-3CT 2 h before the CB-qLuc injection.

Histological Analysis of Collagen Binding in Tumor Tissues. Cy5-labeled CB-Luc (0.5 nmol) was iv injected into the mice with HT1080 tumors. Tumor tissues were collected after 24 h. The frozen tumor tissue samples were stained with a collagen type I primary antibody followed by a secondary antibody labeled with Alexa 488 after washing. Fluorescence images were collected with a Cy5 filter set for the Cy5-labeled CB-Luc and an FITC filter set for immunostained type I collagen.

Histological Analysis of Skin Tissues. The skin samples were collected after imaging, inflated with 4% paraformaldehyde, fixed overnight at 4 °C, and embedded in paraffin. Sections were stained with hemotoxylin and eosin.

Detection of MMP in Skin Tissuse on Zymography. The skin samples were homogenized in 1% Triton-X in PBS with protease inhibitor cocktail added. The protein concentration was measured by BCA assay, and the protein sample (5 μg) was loaded on Novex zymogram gel from Invitrogen. Active MMP-2, Pro-MMP-9 and aminophenyl mercuric acetate activated MMP-9 were used as the standards.

■ ASSOCIATED CONTENT

Ⓢ Supporting Information. Supplementary Figures 1−5 and Supplementary Methods on the preparation of the reporters. This material is available free of charge *via* the Internet at http://pubs.acs.org.

■ AUTHOR INFORMATION

Corresponding Author

*E-mail: jrao@stanford.edu.

Present Address

#Department of Life Science, Hanyang University, Seoul 133-791, Republic of Korea.

■ ACKNOWLEDGMENT

This work was supported by National Institutes of Health grant R01CA135294, the Stanford University National Cancer Institute (NCI) CCNE grant (U54CA119367) and NCI ICMIC (P50CA114747). We are grateful to Professor Agneta Höök at Texas A&M University for the gift of CNA35 plasmid and Drs. Zheng Miao, Hongguang Liu, Frederick Chin, David Dick and Frezghi Habte at Stanford University for technical assistance with the ^{64}Cu labeling and PET image analyses.

■ REFERENCES

(1) Scadden, D. T. (2006) The stem-cell niche as an entity of action. *Nature 441*, 1075–1079.

(2) Fuchs, E., Tumbar, T., and Guasch, G. (2004) Socializing with the neighbors: stem *cells* and their niches. *Cell 116*, 769–778.

(3) Hu, M., and Polyak, K. (2008) Microenvironmental regulation of cancer development. *Curr. Opin. Genetics Dev. 18*, 27–34.

(4) Bissell, M. J., and Radisky, D. (2001) Putting tumors in context. *Nat. Rev. Cancer 1*, 46–54.

(5) Joyce, J. A. (2005) Therapeutic targeting of the tumor microenvironment. *Cancer Cell 7*, 513–520.

(6) Mbeunkui, F., and Johann, D. J., Jr. (2009) Cancer and the tumor microenvironment: A review of an essential relationship. *Cancer Chemother. Pharmacol. 63*, 571–582.

(7) Allinen, M., Beroukhim, R., Cai, L., Brennan, C., Lahti-Domenici, J., Huang, H., Porter, D., Hu, M., Chin, L., Richardson, A., Schnitt, S., Sellers, W. R., and Polyak, K. (2004) Molecular characterization of the tumor microenvironment in breast cancer. *Cancer Cell 6*, 17–32.

(8) Herschman, H. R. (2003) Molecular imaging: looking at problems, seeing solutions. *Science 302*, 605–608.

(9) Provenzano, P. P., Eliceiri, K. W., and Keely, P. J. (2009) Shining new light on 3D cell motility and the metastatic process. *Trends Cell Biol. 19*, 638–648.

(10) Weissleder, R. (2002) Scaling down imaging: molecular mapping of *cancer* in mice. *Nat. Rev. Cancer 2*, 11–18.

(11) Hoffman, R. M. (2005) The multiple uses of fluorescent proteins to visualize cancer in vivo. *Nat. Rev. Cancer 5*, 796–806.

(12) Yang, M., Li, L., Jiang, P., Moossa, A. R., Penman, S., and Hoffman, R. M. (2003) Dual-color fluorescence imaging distinguishes tumor cells from induced host angiogenic vessels and stromal cells. *Proc. Natl Acad. Sci. USA 100*, 14259–14262.

(13) Condeelis, J., and Segall, J. E. (2003) Intravital imaging of cell movement in tumors. *Nat. Rev Cancer 3*, 921–930.

(14) Brown, E. B., Campbell, R. B., Tsuzuki, Y., Xu, L., Carmeliet, P., Fukumura, D., and Jain, R. K. (2001) *In vivo* measurement of gene expression, angiogenesis and physiological function in tumors using multiphoton laser scanning microscopy. *Nat. Med.7*, 864–868.

(15) Zong, Y., Xu, Y., Liang, X., Keene, D. R., Höök, A., Gurusiddappa, S., Höök, M., and Nrayana, S. V. L. (2005) A 'collagen hug' model for *Staphylococcus aureus* CNA binding to collagen. *EMBO J. 24*, 4224–4236.

(16) Krahn, K. N., Bouten, C. V., van Tuijl, S., van Zandvoort, M. A., and Merkx, M. (2006) Fluorescently labeled collagen binding proteins allow specific visualization of collagen in tissues and live cell culture. *Anal. Biochem. 350*, 177–185.

(17) Boerboom, R. A., Krahn, K. N., Megens, R. T., van Zandvoort, M.A., Merkx, M., and Bouten, C. V. (2007) High resolution imaging of collagen organization and synthesis using a versatile collagen specific probe. *J. Struct. Biol. 159*, 392–399.

(18) Megens, R. T., Oude Egbrink, M. G., Cleutjiens, J. P., Kuijpers, M. J., Schiffers, P. H., Merkx, M., Slaaf, D. W., and van Zandvoort, M. A. (2007) Imaging collagen in intact viable healthy and atherosclerotic arteries using fluorescently labeled CNA35 and two-photon laser scanning microscopy. *Mol. Imaging 6*, 247–260.

(19) Loening, A. M., Fenn, T. D., Wu, A. M., and Gambhir, S. S. (2006) Consensus guided mutagenesis of Renilla luciferase yield enhanced stability and light output. *Protein Eng. Des. Sel. 19*, 391–400.

(20) Loening, A. M., Wu, A. M., and Gambhir, S. S. (2007) Red-shifted *Renilla reniformis* luciferase for imaging in living subjects. *Nat. Methods 4*, 641–643.
(21) Egeblad, M., and Werb, Z. (2002) New functions for matrix metalloproteinases in cancer progression. *Nat. Rev. Cancer 2*, 161–174.
(22) Scherer, R. L., McIntyre, J. O., and Matrisian, L. M. (2008) Imaging matrix metalloproteinases in cancer. *Cancer Metastasis Rev. 27*, 679–690.
(23) Weissleder, R., Tung, C. H., Mahmood, U., and Bogdanov, A., Jr. (1999) In vivo imaging of tumors with protease-activated near-infrared fluorescent probes. *Nat. Biotechnol. 17*, 375–378.
(24) Jiang, T., Olson, E. S., Nguyen, Q. T., Roy, M., and Jennings, P. A. (2004) Tumor imaging by means of proteolytic activation of cell-penetrating peptides. *Proc. Natl. Acad. Sci. U.S.A. 101*, 17867–17872.
(25) McIntyre, J. O., Fingleton, B., Wells, K. S., Piston, D. W., Lynch, C. C., Gautam, S., and Matrisian, L. M. (2004) Development of a novel fluorogenic proteolytic beacon for *in vivo* detection and imaging of tumour-associated matrix metalloproteinase-7 activity. *Biochem. J. 377*, 617–628.
(26) Prinz, A., Erlbruch, A., and Herberg, F. W. (2004) Monitoring cAMP dependent protein kinase subunit interaction in intact cells using bioluminescence resonance energy transfer (BRET). *FASEB J. 18*, C159–C160.
(27) So, M.-K., Xu, C., Loening, A. M., Gambhir, S. S., and Rao, J. (2006) Self-illuminating quantum dot conjugates for in vivo imaging. *Nat. Biotechnol. 24*, 339–343.
(28) Xia, Z., and Rao, J. (2009) Biosensing and imaging based on bioluminescence resonance energy transfer. *Curr. Opin. in Biotechnol. 20*, 37–44.
(29) Brown, S., Bernardo, M. M., Li, Z.-H., Kotra, L. P., Tanaka, Y., Fridman, R., and Mobashery, S. (2000) Potent and selective mechanism-based inhibition of gelatinases. *J. Am. Chem. Soc. 122*, 6799–6800.
(30) Olsen, E., Aguilera, T. A., Jiang, T., Ellies, L. G., Nguyen, Q. T., Wong, E., Gross, L., and Tsien, R. Y. (2009) In vivo characterization of activatable cell penetrating peptides for targeting protease activity in cancer. *Integr. Biol. 1*, 382–393.
(31) Xia, Z., Xing, Y., So, M.-K., Koh, A. L., Sinclair, R., and Rao, J. (2008) Multiplex detection of protease activity with quantum dot nanosensors prepared by intein-mediated specific bioconjugation. *Anal. Chem. 80*, 8649–8655.
(32) Stahtea, X. N., Roussidis, A. E., Kanakis, I., Tzanakakis, G. N., Chalkiadakis, G., Mavroudis, D., Kletsas, D., and Karamanos, N. K. (2007) Imatinib inhibits colorectal cancer cell growth and suppress stromal-induced growth stimulation, MT1-MMP expression and pro-MMP-2 activation. *Int. J. Cancer 121*, 2808–2814.
(33) Gambhir, S. S. (2002) Molecular imaging of cancer with positron emission tomography. *Nat. Rev. Cancer 2*, 683–693.
(34) Nathan, C. (2002) Points of control in inflammation. *Nature 420*, 846–852.
(35) Degushi, J. O., Aikawa, M., Tung, C. H., Aikawa, E., Kim, D. E., Ntziachristos, V., Weissleder, R., and Libby, P. (2006) Inflammation in atherosclerosis: visualizing matrix metalloproteinase action in macrophages in vivo. *Circulation 114*, 55–62.
(36) Stanley, P. L., Steiner, S., Havens, M., and Tramposch, K. M. (1991) Mouse skin inflammation induced by multiple topical application of 12-O-tetradecanoylphorbol-13-acetate. *Skin Pharmacol. 4*, 262–271.
(37) Opdenakker, G., Van den Steen, P. E., Dubois, B., Nelissen, I., Van Coillie, E., Masure, S., Proost, P., and Van Damme, J. (2001) Gelatinase B functions as regulators and effectors in leukocyte biology. *J. Leukoc. Biol. 69*, 851–9.
(38) Parks, W. C., Wilson, C. L., and López-Boado, Y. S. (2004) Matrix matelloproteinases as modulators of inflammation and innate immunity. *Nat. Rev. Immunol. 4*, 617–629.
(39) Ra, H. J., and Parks, W. C. (2007) Control of matrix metalloproteinase catalytic activity. *Matrix Biol. 26*, 587–596.
(40) Jiang, Y., Goldberg, I. D., and Shi, Y. E. (2002) Complex roles of tissue inhibitors of metalloproteinases in cancer. *Oncogene 21*, 2245–52.
(41) Van Duijnhoven, S. M. J., Robillard, M. S., Nicolay, K., and Grüll, H. (2011) Tumor targeting of MMP-2/9 activatable cell-penetrating imaging probes is caused by tumor-independent activation. *J. Nucl. Med. 52*, 279–286.
(42) Hayakawa, T., Yamashita, K., Tanzawa, K., Uchijima, E., and Iwata, K. (1992) Growth-promoting activity of tissue inhibitor of metalloproteinases-1 (TIMP-1) for a wide range of cells. A possible new growth factor in serum. *FEBS Lett. 298*, 29–32.
(43) Li, G., Fridman, R., and Kim, H. R. (1999) Tissue inhibitor of metalloproteinase-1 inhibits apoptosis of human breast epithelial cells. *Cancer Res. 59*, 6267–75.
(44) Wang, Z., Juttermann, R., and Soloway, P. D. (2000) TIMP-2 is required for efficient activation of proMMP-2 in vivo. *J. Biol. Chem. 275*, 26411–26415.
(45) Loening, A. M., and Gambhir, S. S. (2003) AMID: a free software tool for multimodality medical image analysis. *Mol. Imaging 2*, 131–137.